J. Fluid Mech. (1989), vol. 201, pp. 223–242
Printed in Great Britain

Growth of radial viscous fingers in a Hele-Shaw cell

By JING-DEN CHEN
Mead Imaging, 3385 Newmark Drive, Miamisburg, OH 45342, USA

(Received 16 October 1987 and in revised form 16 August 1988)

A series of experiments are performed in a Hele-Shaw cell, consisting of two parallel closely spaced glass plates. A liquid (oil or water, both of viscosity of 1.0 cP) is injected at a constant volumetric flow rate, q, to radially displace a much more viscous liquid (glycerine, 1050 cP) in the cell. Oil is immiscible with and water is miscible with glycerine. The data presented in this paper are taken mostly at late stages of the fingering process, when the pattern has multiple generations of splitting. Correlations with time are obtained for the finger length and the overall pattern density. The time- and lengthscales have been found for the immiscible case. At the same dimensionless time, immiscible patterns are similar and have the same generation of splitting. The overall density of each pattern decreases with time. The pattern shows fractal behaviour only after a certain number of generations of splitting. The fractal dimension of the immiscible pattern decreases from 1.9 to 1.82 when the pattern goes from the third to the sixth generation of splitting. The fractal dimension of the miscible pattern reaches a constant value after about ten generations of splitting and the fractal dimension ranges from 1.50 to 1.69 for $q/Db = 4.8 \times 10^5$–7.0×10^6. The miscible patterns are insensitive to dispersion for large q/Db. For immiscible fingers λ/b scales with $Ca^{-0.31}$ for capillary number Ca ranging from about 8×10^{-4} to 0.05. For miscible fingers, λ/b is insensitive to dispersion and ranges from 5 to 10 for large q/Db. Here D is the molecular diffusion coefficient in glycerine, b the cell gap width and λ the splitting wavelength.

1. Introduction

A Hele-Shaw (1898) cell consists of two closely spaced plane parallel plates. It has been used as an analogue of two-dimensional isotropic homogeneous porous media for studying viscous fingering problems (Saffman & Taylor 1958; Chouke, van Meurs & van der Poel 1959; Benham & Olson 1963; Stalkup 1984; Homsy 1987). When a less viscous fluid displaces a more viscous one, the boundary between the fluids is usually uneven and the less viscous fluid 'fingers' into the more viscous one. Once the less viscous fluid breaks through the porous medium, much of the resident fluid is left behind. This unstable phenomenon, resulting in an inefficient displacement, has been observed in laboratory systems (van Meurs 1957; Blackwell, Rayne & Terry 1959).

Viscous fingering in a Hele-Shaw cell has been used to study the acidizing pattern in the fracture of an oil reservoir. To increase the oil production rate, the pay zone of an oil reservoir is sometimes hydraulically fractured by pumping a viscous fluid into the oil well. To prevent the closure of fracture, permanent flow channels can be created by injecting acid into the newly fractured reservoir to etch the walls of the

fracture (Howard & Fast 1970). The flow pattern of the injected acid in the fracture will determine the channel pattern on the walls.

For these processes it is important to know the size and speed of fingers and the coverage of the fingering pattern. Although the Hele-Shaw cell does not contain some important features of a porous medium or the fracture of a porous medium, understanding the fingering process in a well-defined geometry should help us attack the more complex problems. Many studies have been reported on viscous fingering in Hele-Shaw cells and in porous media. For a good review on these subjects, see Homsy (1987). In this paper we are interested in the dynamics of radial viscous fingers which is related to the problems stated above.

Many studies have been reported on the radial viscous fingering in a Hele-Shaw cell. Paterson (1981, 1985) has studied the linear stability of a circular interface evolving into fingers. Using numerical calculations, Howison (1986) has shown some symmetrical immiscible fingering patterns similar to those reported by Paterson (1981). Chen (1987) has studied the qualitative effects of flow rate and plate roughness on the radial miscible and immiscible fingering patterns. Daccord, Wittman & Stanley (1986) have measured the fractal dimension and the finger width for water fingers developed in an aqueous non-Newtonian fluid. Rauseo, Barnes & Maher (1987) have studied the fractal dimension and the length- and timescales of radial immiscible fingering patterns.

In this paper we investigate experimentally the following problems, emphasizing the fingering process at late stages when the pattern has multiple generations of splitting. What is the effect of flow rate on the fingering pattern? What is the relationship between the finger length and time? What are the lengthscale and the timescale in a radial flow geometry? How does the pattern density change with time? When does the pattern become a fractal? What is the relationship between the splitting wavelength of a finger and its speed?

2. Experiments

The experimental system and procedure are the same as those described for a smooth Hele-Shaw cell by Chen (1987). The cell is made by using two smooth glass plates of $0.55 \times 10 \times 10$ cm with four plastic shims of 75 ± 2 μm in thickness clamped between the plates at the four corners by binder clips. The plate has a flatness of less than 5 μm across the 10×10 cm surface and a roughness of less than 0.04 μm. The top plate has a small hole (0.17 cm in diameter) drilled in the centre for injecting the fluids. The four shims of 2.5×3.2 cm are cut from one long piece and three measurements of thickness are made on each with a micrometer. Each shim is placed near each corner of the bottom plate with its long side perpendicular to the diagonal of the plate and the midpoint of one long side over the corner of the plate. The top plate is then placed on top of the four shims and aligned with the bottom plate and four binder clips clamp the plates.

To improve visualization, the displacing fluids are dyed blue. Two different types of displacement experiments are: (*a*) dyed oil displacing glycerine, and (*b*) dyed water displacing glycerine. Type (*a*) is immiscible, and (*b*) is miscible.

Three different flow rates are used for type (*a*): $q = 1.40 \times 10^{-4}$, 5.35×10^{-4} and 2.03×10^{-3} ml/s. To check the reproducibility of the experiment, each flow rate is run twice. For type (*b*) five different flow rates are used: $q = 7.12 \times 10^{-5}$, 1.40×10^{-4}, 5.35×10^{-4}, 7.50×10^{-4} and 1.05×10^{-3} ml/s. Only the third flow rate is run twice to check the reproducibility. In type (*a*) the glycerine wets the glass plate. The

interfacial tension, γ, between dyed oil and glycerine is 20.0 dyn/cm. The viscosity of the displacing phase μ_i is 1.0 cP, and that of glycerine $\mu = 1050 \pm 30$ cP. The viscosity contrast ratio, $\mu - \mu_i / \mu + \mu_i$, is 1 in both cases. The glycerine has a density $\rho = 1.26$ gm/cm^3. The densities of dyed water and dyed oil are 1.0 and 0.74 gm/cm^3, respectively. All experiments are run at room temperature, 24.0° to 24.5 °C.

The dry cell is set horizontally, then the glycerine is injected through the central hole in the top plate until it fills most of the flow space in the cell. Since the displacement of air by glycerine is stable, a circular interface is formed. The displacing fluid is then injected by a syringe pump at a selected constant volumetric flow rate. In the miscible case the flow rates are high enough that the molecular diffusion of dye into glycerine is negligible. The displacement process is recorded as time-sequence photographs by a 35 mm camera. Taking advantage of the circular interface formed by injecting glycerine into an empty cell, we can measure the gap width of the cell. The area invaded by glycerine injected at a constant flow rate is measured as a function of time from time-sequence photographs. Two flow rates are used for this purpose: $q = 1.40 \times 10^{-4}$ and 2.03×10^{-3} ml/s. The calculated gap width is found to be 75 ± 2 μm for both flow rates. This indicates that there is no bending in the cell.

3. Results and discussion

For the immiscible case the dimensionless flow rate, $\mu q / \gamma b^2$, ranges from 1.30 to 19.0, the capillary number, $Ca \equiv \mu V / \gamma$, from about 10^{-3} to 10^{-1}, and the Reynolds number, $\rho V b / \mu$, from about 10^{-6} to 10^{-4}. Here b is the gap width of the cell and V is the finger speed, as defined in §3.4. For the miscible case, the dimensionless flow rate, q/Db, ranges from 4.8×10^5 to 7.0×10^6, the Péclet number, bV/D, from 10^3 to 10^5, and the Reynolds number from 10^{-6} to 10^{-4}. Here we assume the molecular diffusion coefficient, D, in glycerine to be 2×10^{-8} cm^2/s. (The self-diffusion coefficient of glycerine at 24 °C is 2×10^{-8} cm^2/s (Burnett & Harmon 1972).) (Strictly speaking, Taylor dispersion plays an important role in miscible experiments, and the correct definition of the Péclet number should be based on some measure of the dispersion coefficient not the molecular diffusion coefficient. Here we use the molecular diffusion coefficient as a reference value of the dispersion coefficient (Homsy 1987).) Note that these values are estimated based on the properties of the more viscous fluid.

3.1. *Qualitative observations*

For the immiscible case at low flow rate, $\mu q / \gamma b^2 \equiv 1.30$, the fluid boundary initially expands, becomes wavy and splits to form first-generation fingers. Owing to the radial geometry, these fingers spread and develop into a fan shape as they grow, and some of them split to form second-generation fingers when the width is big enough. This cascading process of finger splitting is shown in figure 1 (*a*), which is an overlay of digitized images of nine selected time-sequence photographs. Owing to the finite size of the cell, only two generations of fingers are possible at this low dimensionless flow rate. As the flow rate increases, the fingers split more frequently at a narrower width. Third and sixth generations of splitting occur within the sample at $\mu q / \gamma b^2 =$ 4.99 and 19.0, respectively, as shown in figures 1 (*b*) and 1 (*c*). The shielding of small fingers by large ones can be seen in figures 1 (*b*) and 1 (*c*). Spreading, splitting and shielding have been discussed in detail by Homsy (1987) as the three basic growth mechanisms of both miscible and immiscible fingering processes. These patterns seem

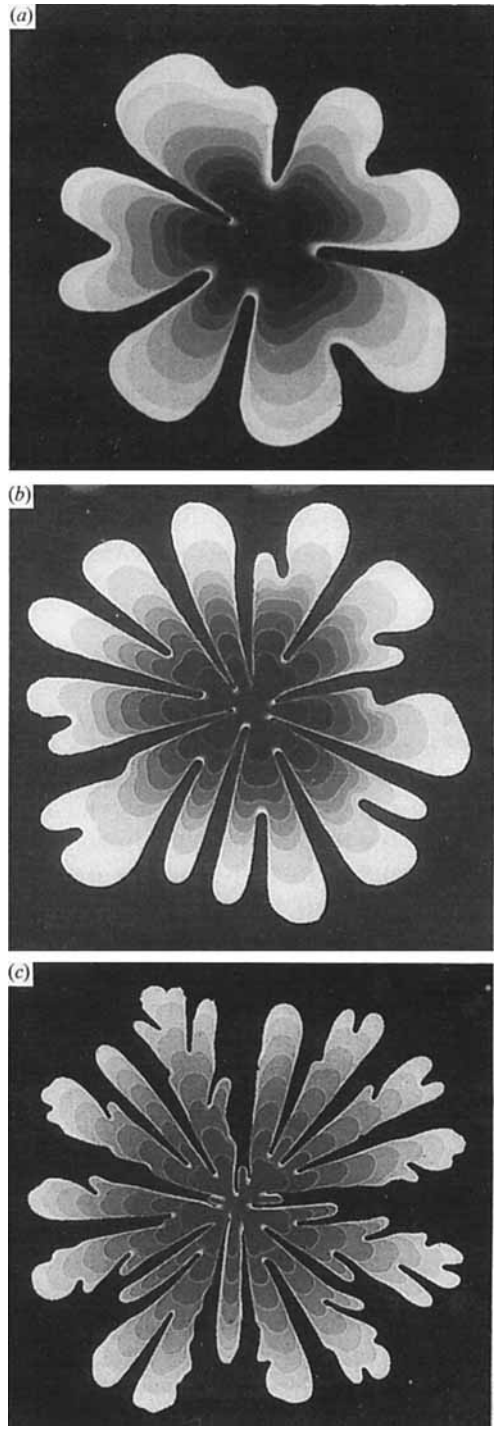

FIGURE 1. Overlays of digitized images of selected time-sequence photographs showing the evolution of immiscible fingering patterns at three different flow rates. Different shadings indicate different times. (*a*) $q = 1.40 \times 10^{-4}$ ml/s ($\mu q/\gamma b^2 = 1.30$), at $t = 37$, 157, 277, 397, 517, 758, 1058, 1358 and 1658 s. (*b*) $q = 5.35 \times 10^{-4}$ ml/s ($\mu q/\gamma b^2 = 4.99$), at $t = 42$, 82, 122, 162, 202, 242, 343 and 493 s. (*c*) $q = 2.03 \times 10^{-3}$ ml/s ($\mu q/\gamma b^2 = 19.0$), at $t = 11$, 19, 27, 35, 43, 51, 59 and 67 s.

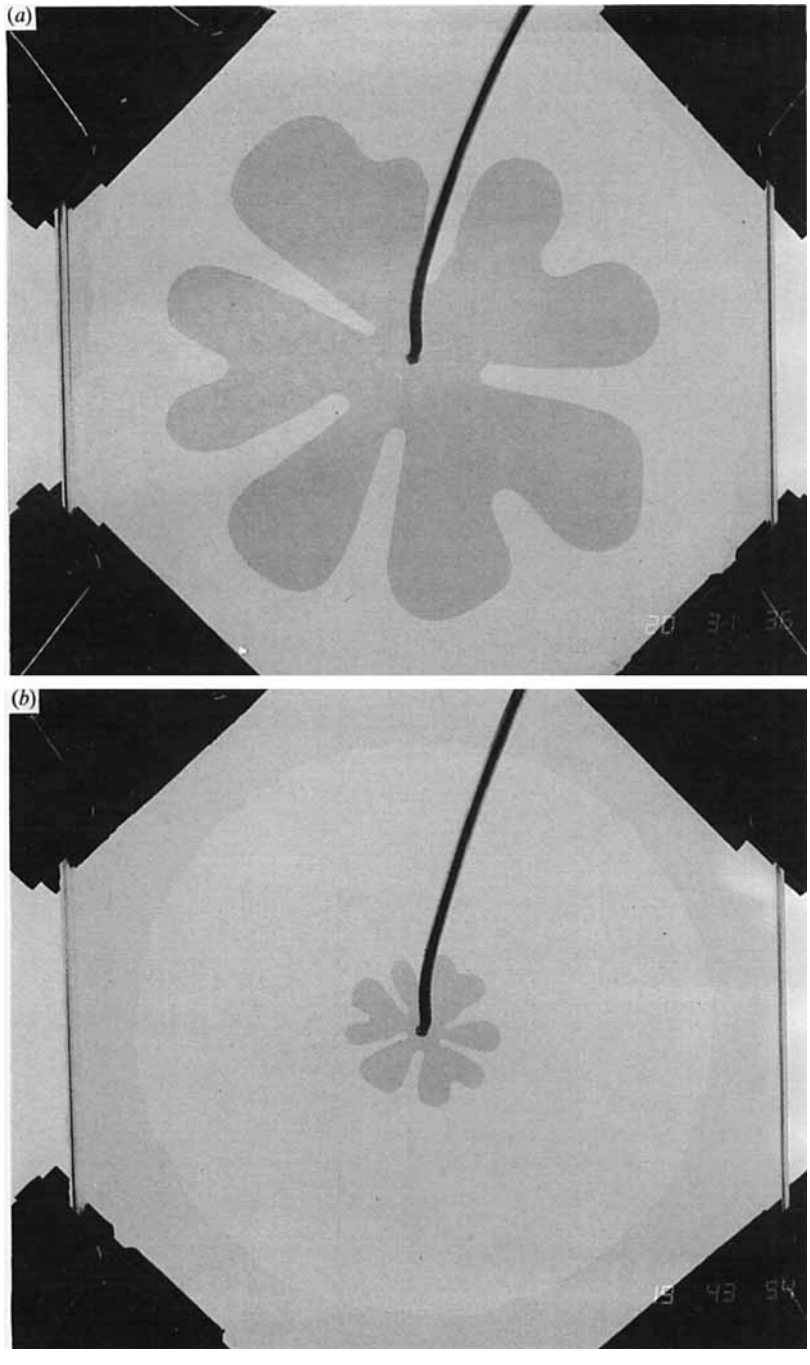

FIGURE 2. (*a*) Original photograph of the last pattern of figure 1 (*a*), and (*b*) that of the first pattern of figure 1 (*b*). Note the geometrical similarity between the two patterns. The former has a dimensionless longest finger length $R_t = 690$ at dimensionless time $T = 9.3 \times 10^5$, and the latter has a dimensionless longest finger length $R_t = 712$ at dimensionless time $T = 1.3 \times 10^6$. The thick dark line in the photographs is the fluid injection tube with a 0.17 cm outside diameter.

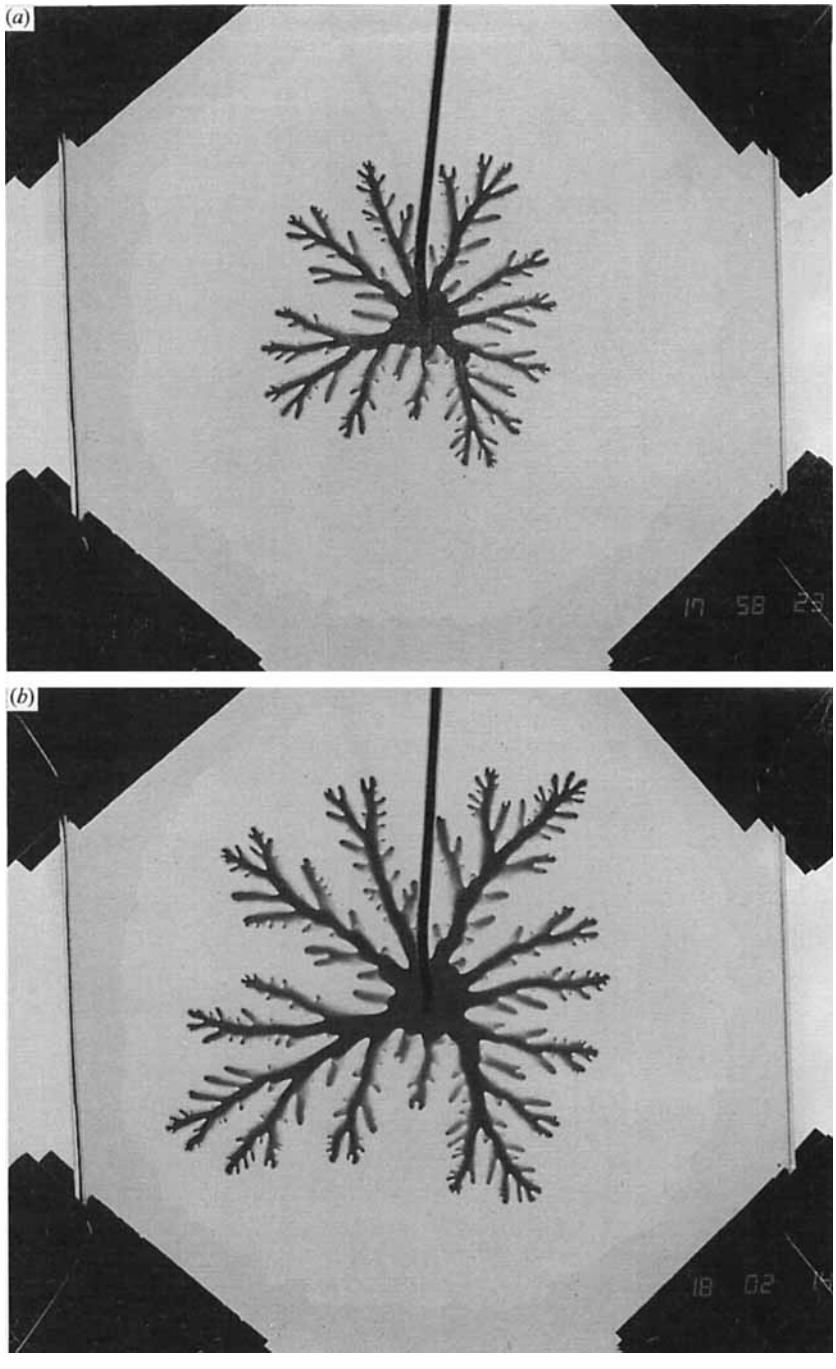

FIGURE 3. Miscible patterns at flow rate $q = 1.40 \times 10^{-4}$ ml/s ($q/Db = 9.3 \times 10^5$) at (*a*) 228 s and (*b*) 459 s, showing thinner water layers at the bases of side fingers and along the boundary of the pattern, and widening of the branches. The thick dark line is the fluid injection tube.

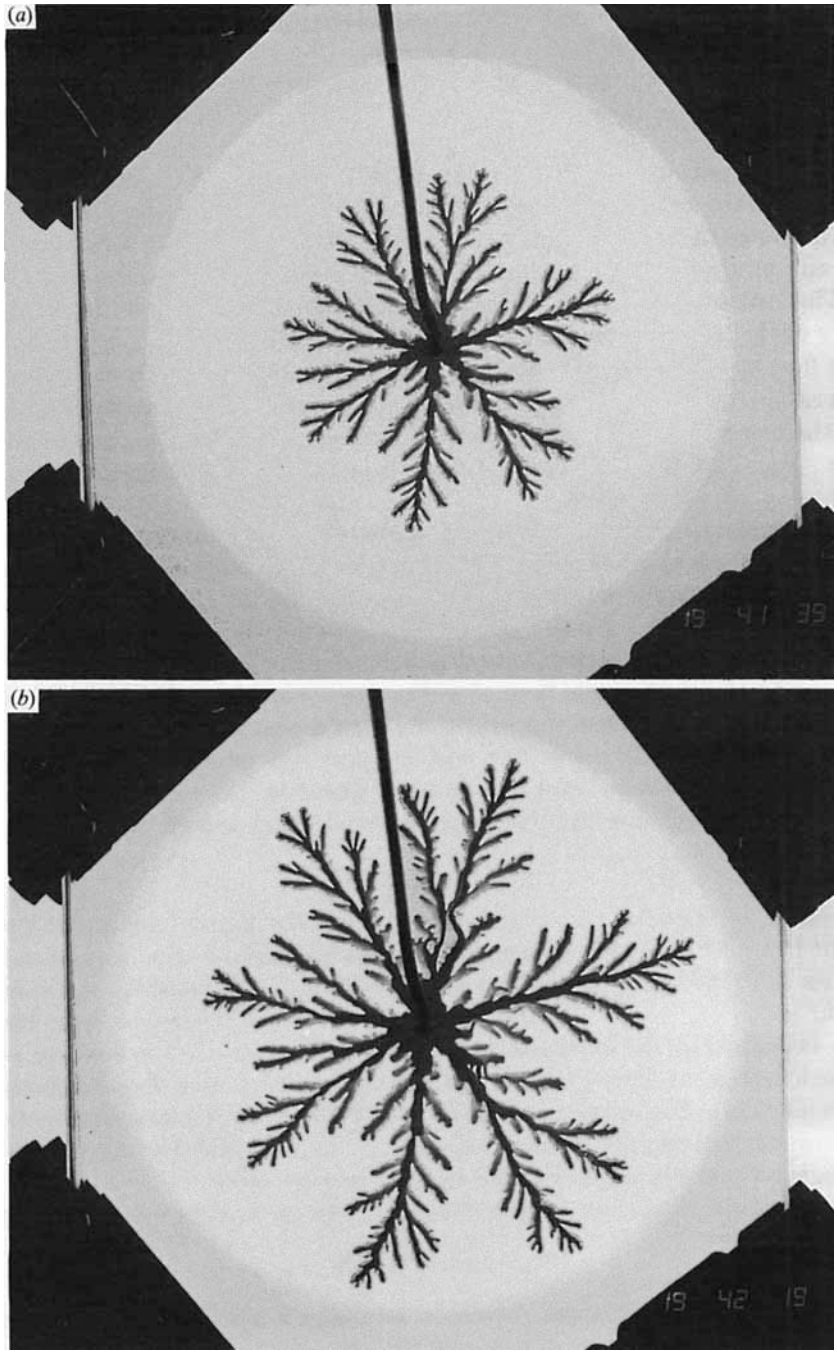

FIGURE 4. Miscible patterns at flow rate $q = 7.50 \times 10^{-4}$ ml/s ($q/Db = 5.0 \times 10^{6}$) at (*a*) $t = 42$ s and (*b*) 82 s, showing thinner water layers at the bases of side fingers and along the boundary of the pattern, widening of the branches and interpenetration of fingers.

to be geometrically similar at the same generation of splitting. For example, we can see that the last pattern in figure 1 (*a*) is similar to the first in figure 1 (*b*), both at the second generation of splitting. The original photographs of these two patterns are shown in figure 2 (the injection tube has been removed from the digitized images shown in figure 1). We shall discuss this similarity in more detail in §3.2.

The fingering pattern formed at the same flow rate is not exactly the same each time for either the miscible or immiscible case. Owing to the absence of interfacial tension, the miscible finger is not of uniform thickness, as can be seen from the non-uniform colour strength in the photographs shown in figures 3 and 4 (see also, Chen 1987). The colour is weaker (brighter in black-and-white pictures) along the boundary of the pattern, indicating a thinner water layer there. This is more obvious at higher flow rates. Also, the bases of some side fingers shielded from further growth have a weaker colour because when they cease to grow, no more dyed water flows through the bases. There are 'loops' in the fingering pattern at flow rates higher than 5.35×10^{-4} ml/s, as shown in figure 4, resulting from interpenetration between the fingers.

There is not much difference in the global structure of miscible patterns at different flow rates, as can be seen by comparing figures 3 and 4. This means that the miscible patterns are insensitive to dispersion for the dimensionless flow rates tested, $q/Db = 4.8 \times 10^5$–7.0×10^6. In §3.4 we shall show that the splitting wavelength of miscible fingers is also insensitive to dispersion for the flow rates tested. For all flow rates, owing to the continuous flow of water, the size of branch increases with time and is bigger near the centre than near the tip, as shown in figures 3 and 4. The growth mechanisms discussed in this and the previous paragraph, i.e. non-uniform thickness, interpenetration and loops, and growing branch width, cannot be described by the diffusion-limited aggregation (DLA) model (Witten & Sander 1983).

3.2. *Finger length*

In this section we consider the correlation between the finger length and time. it is hoped that if we can find such a correlation, then we shall be able to predict how far the pattern will reach at a given time under various experimental conditions, such as different gap, flow rate or physical properties of fluids. For each finger the finger length, r_t, is defined as the distance from the injection point to the farthest point on its tip. The length is measured with a digital vernier micrometer. The maximum error of measurement is $\pm 2\%$ of the average value of three repeated measurements. From the sequence of photographs of each experiment we first identify the fingers on the last photograph and then follow them in time-reverse order.

For the immiscible case the finger length r_t can be expressed as a function of relevant quantities

$$r_t = r_t(1, b, \gamma, \mu, t).$$

Using a dimensional analysis, this can be rearranged in a different form containing three dimensionless groups

$$F\left(\frac{r_t}{b}, \frac{qt}{b^3}, \frac{\mu q}{\gamma b^2}\right) = 0.$$

The equation suggests that if we plot r_t/b against qt/b^3, there will be some correlation between these values with $\mu q/\gamma b^2$ as a parameter. Figure 5 shows such a plot for the data of the longest finger of the first run of the three different flow rates. Although the data roughly fall onto a straight line in a log–log plot, it is desirable to include the parameter $\mu q/\gamma b^2$ in the coordinates.

Assuming that the length- and timescales are related to some power of $\mu q/\gamma b^2$, the above equation can be rearranged as

$$F\left(\frac{r_t}{b}\left[\frac{\mu q}{\gamma b^2}\right]^{\alpha}, \frac{qt}{b^3}\left[\frac{\mu q}{\gamma b^2}\right]^{\beta}\right) = 0.$$

By non-dimensionalizing the governing equations for Hele-Shaw flows,

$$\boldsymbol{v} = -\frac{b^2}{12\mu}\nabla p$$

and

$$p_i - p = \gamma\kappa,$$

we find $\beta = 3\alpha - 1$. Here κ is the curvature of interface, p_i is the pressure of the displacing fluid, p and $\boldsymbol{v}$ are the two-dimensional gap-averaged pressure and velocity fields in the displaced fluid, respectively. To find the value of α we plot $(r_t/b)[\mu q/\gamma b^2]^{\alpha}$ against $(qt/b^3)[\mu q/\gamma b^2]^{\beta}$ for the longest finger of each experiment using different values of α. For $\alpha = 1$ we find that the data points roughly fall onto one straight line, as shown in figure 6. Data of two runs at each flow rate shown in the figure indicate the reproducibility of the experiment. The dashed line in figure 6 represents the least-square-fit to the data.

$$R_t = 0.32T^{0.55}. \tag{1}$$

Here

$$R_t \equiv \frac{r_t}{r_0} \tag{2}$$

and

$$T \equiv \frac{t}{t_0}. \tag{3}$$

This means that during the growth of the radial fingering pattern the lengthscale r_0 and timescale t_0 are

$$r_0 = b\left[\frac{\mu q}{\gamma b^2}\right]^{-1} \tag{4}$$

and

$$t_0 = \frac{b^3}{q}\left[\frac{\mu q}{\gamma b^2}\right]^{-2}. \tag{5}$$

In figures 5 and 6 the data for the highest flow rate show an increase in slope. This indicates perhaps a change in fingering mechanism as the flow rate increases. This mechanism may be connected to increases in the wetting film thickness and the finger tip curvature. As the flow rate increases, both the wetting film thickness behind the finger and the finger tip curvature increase. Tabeling, Zocchi & Libchaber (1987) have studied the wetting film thickness and the Saffman–Taylor instability in a linear cell. They indicate that the wetting film has a stabilizing effect on the finger. Kopf-Sill & Homsy (1988) have shown that the tip curvature stabilizes the finger in a linear cell. In §3.4 we also observe the stabilizing effect of tip curvature. It is not clear how these stabilizing effects affect the change in the slope of our data. It is also interesting to note that Kopf-Sill & Homsy find no fractal fingering in a linear cell. In §3.3 we find fractal fingering at the highest flow rate.

Rauseo *et al.* (1987) use the same scalings as shown in (4) and (5) and plot the scaled perimeter length of fingering patterns against the scaled time for experiments with $b = 0.10$, 0.15 and 0.24 cm. They find that the data do not collapse onto one curve and suggest that there may be some dependence on b through the wetting film effect.

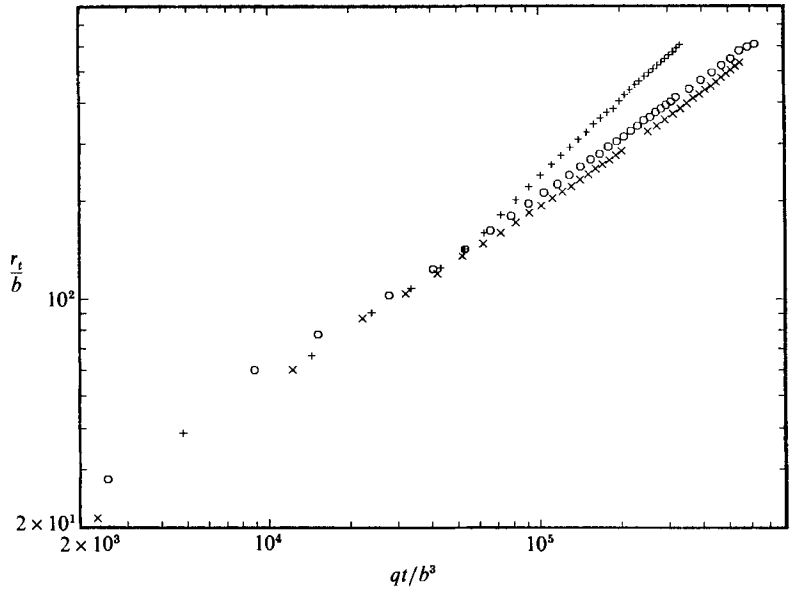

FIGURE 5. Data of (r_t/b) versus (qt/b^3) for the longest finger of first run at $\mu q/\gamma b^2 = 1.30$ (×), 4.99 (○) and 19.0 (+).

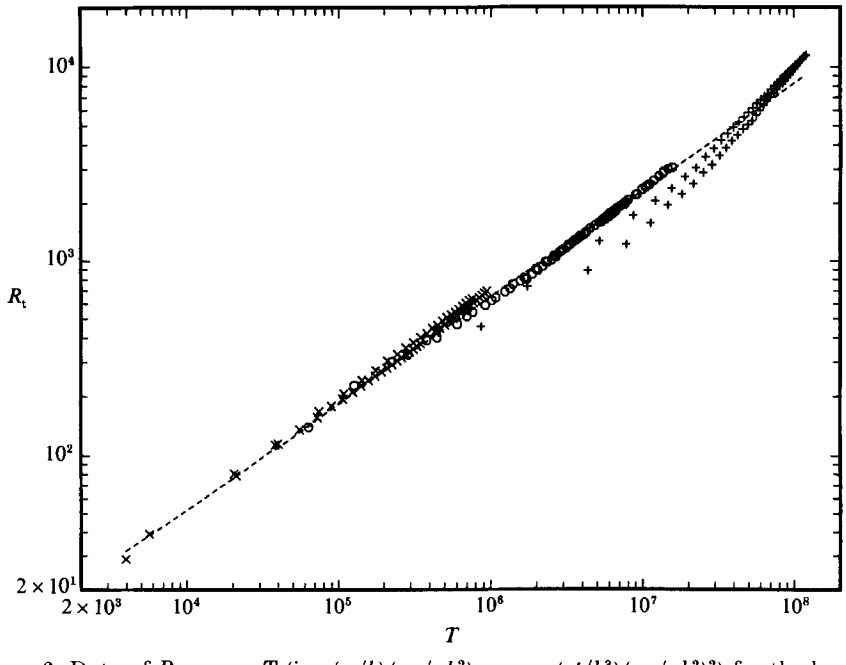

FIGURE 6. Data of R_t versus T (i.e. $(r_t/b)(\mu q/\gamma b^2)$ versus $(qt/b^3)(\mu q/\gamma b^2)^2$) for the longest finger of two runs at each flow rate, $\mu q/\gamma b^2 = 1.30$ (×), 4.99 (○) and 19.0 (+). Dashed line represents equation (1).

(See (18) below for a more appropriate boundary condition proposed by Park & Homsy 1984.) Unfortunately, the values of q and Ca are not reported along with the data. In our experiments $b = 0.0075$ cm, which is one order of magnitude smaller than their b. Further experiments are needed to check whether the scales are dependent on b.

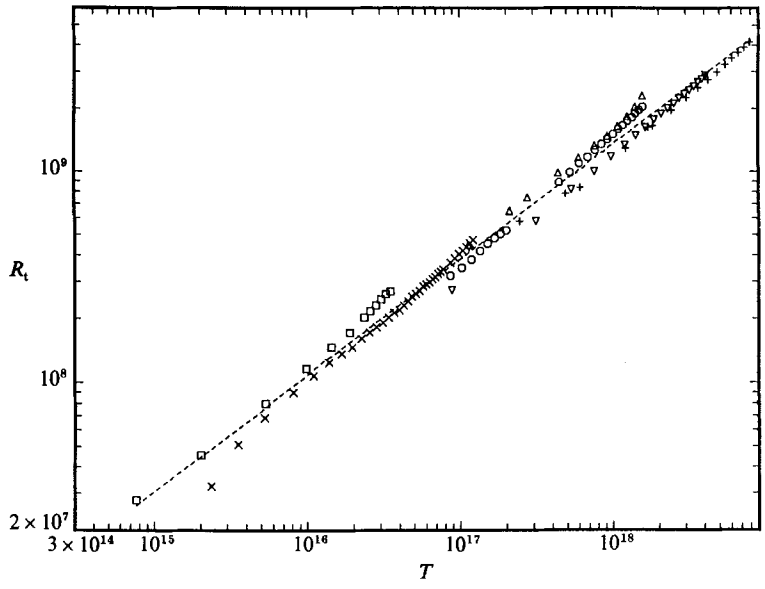

FIGURE 7. Data of R_t versus T (i.e. $(r_t/b)(q/Db)$ versus $(qt/b^3)(q/Db)^2$) for the longest finger of five flow rates $q/Db = 4.75\times10^5$ (□), 9.3×10^5 (×), 3.57×10^6 (○, △), 5.0×10^6 (▽), 7.0×10^6 (+). Dashed line represents equation (8).

In §3.1 we pointed out that there is some geometrical similarity between the two patterns shown in figure 2. Now let us compare these fingering patterns in terms of the length- and timescales. Both patterns are at the stage of second-generation splitting. The dimensionless length and time are given in the captions of figure 2. The closeness of the dimensionless lengths and times and the geometrical similarity between the patterns by visual inspection confirm that (4) and (5) are the right scalings. This means that in terms of these scales both patterns are roughly of the same size and 'age'. This also suggests that the generation of splitting is a good indication of the 'age' of the pattern.

Similarly, for the miscible case we have

$$r_t = r_t(q, b, D, t), \tag{6}$$

which can be rearranged as

$$F\left(\frac{r_t}{b}\left[\frac{q}{Db}\right]^{\alpha}, \frac{qt}{b^3}\left[\frac{q}{Db}\right]^{\beta}\right) = 0. \tag{7}$$

We find that for $\alpha = 1$ and $\beta = 2$ the data points of R_t versus T for the longest fingers of five different flow rates roughly fall onto a straight line, as shown in figure 7. The dashed line represents the least-square-fit to the data,

$$R_t = 0.18T^{0.55}. \tag{8}$$

Here R_t and T are defined similarly as for the immiscible case with

$$r_0 = b\left[\frac{q}{Db}\right]^{-1} \tag{9}$$

and

$$t_0 = \frac{b^3}{q}\left[\frac{q}{Db}\right]^{-2}. \tag{10}$$

The closeness of the data from two runs at flow rate $q = 5.35\times10^{-4}$ ml/s indicates the reproducibility of experiments.

3.3. *Density of finger pattern*

To investigate the evolution of the density of fingering pattern, we digitize the time-sequence photographs of each experiment and plot the density of each pattern as a function of normalized radius r_n. The normalized radius r_n is defined as the radius r divided by the radius of the longest finger in each pattern. The density d is defined as the ratio of the area occupied by the pattern within a radius r to πr^2. The pixel size of digitization is 0.01×0.01 cm.

Figures 8(*a*), 8(*b*) and 8(*c*) show the evolution of d–r_n curves of the immiscible fingering patterns shown in figures 1(*a*), 1(*b*) and 1(*c*), respectively. Each d–r_n curve corresponds to each pattern shown in the respective figure. As time increases the d–r_n curve shifts towards the lower-left corner of the plot. From these plots we see that the density of the fingering pattern decreases with time. At $\mu q/\gamma b^2 = 1.3$ when the first-generation fingers just begin to form the pattern is very compact, so most of the d–r_n curve is close to $d = 1$, as shown in figure 1(*a*). Comparison of these plots of different flow rates shows that there is some similarity in the d–r_n curves for patterns at the same generation of splitting. Indeed, the last curve in figure 8(*a*) has a similar shape to the first one in figure 8(*b*). This is consistent with the geometrical similarity between the last pattern of figure 1(*a*) and the first pattern of figure 1(*b*), both at the secondary splitting stage, as discussed in §3.2 and shown in figures 2(*a*) and 2(*b*). This suggests that if the cell is big enough to allow for further splitting, the pattern formed at low values of $\mu q/\gamma b^2$ will be similar to that formed at high values.

As the number of splittings increases, the intermediate portion of the d–r_n curve of the pattern becomes a straight line in a log–log plot with slope $-\alpha$. In our experiments, only at the highest flow rate did a significant portion of the curve become close to a straight line. This is because at low flow rates there is not enough splitting and the size of the finger is comparable with the size of the pattern. Figure 9 shows that for $\mu q/\gamma b^2 = 19.0$ the value of the fractal dimension (Mandelbrot 1983), $2-\alpha$, decreases from about 1.9 to 1.82 as qt/b^3 increases from about 9×10^4 to 3×10^5. From figures 1(*c*) and 9 we see that the value of $2-\alpha$ decreases from 1.9 to 1.82 when the pattern goes from the third to the sixth generation of splitting. Rauseo *et al.* (1987) report that the value of $2-\alpha$ ranges from 1.69 to 1.92 for $\mu q/\gamma b^2$ ranging from 3 to 16. They find that there is no apparent dependence of $2-\alpha$ on $\mu q/\gamma b^2$. This can be explained by our observation that the value of $2-\alpha$ depends on the growth time. It is obvious that $2-\alpha$ equals 2 when the interface is a circle, and as the fingers develop it will have a value between 1 and 2. From this we can argue that $\mu q/\gamma b^2$ is not the only parameter controlling the value of $2-\alpha$ and that the value should also be dependent upon the time (or the generation of splitting). Unfortunately, the time is not reported along with the value of $2-\alpha$ in their paper. Further experiments are needed to check whether $2-\alpha$ approaches some constant as the number of splittings ('age') increases, and whether the constant is independent of the flow rate. For miscible fingering patterns we find that the value of $2-\alpha$ approaches some constant as the number of splittings ('age') increases. This is reported later in this section.

In figure 10 we plot the overall density d_1, the density d at $r_n = 1$, of each pattern at different flow rates as a function of $(qt/b^3)(\mu q/\gamma b^2)$. Data of two runs at each flow rate are given, showing that d_1 decreases with time. The dashed line represents the least-square-fit to the data,

$$d_1 = 1.25 - 0.048 \ln\left(\frac{qt}{b^3}\frac{\mu q}{\gamma b^2}\right). \tag{11}$$

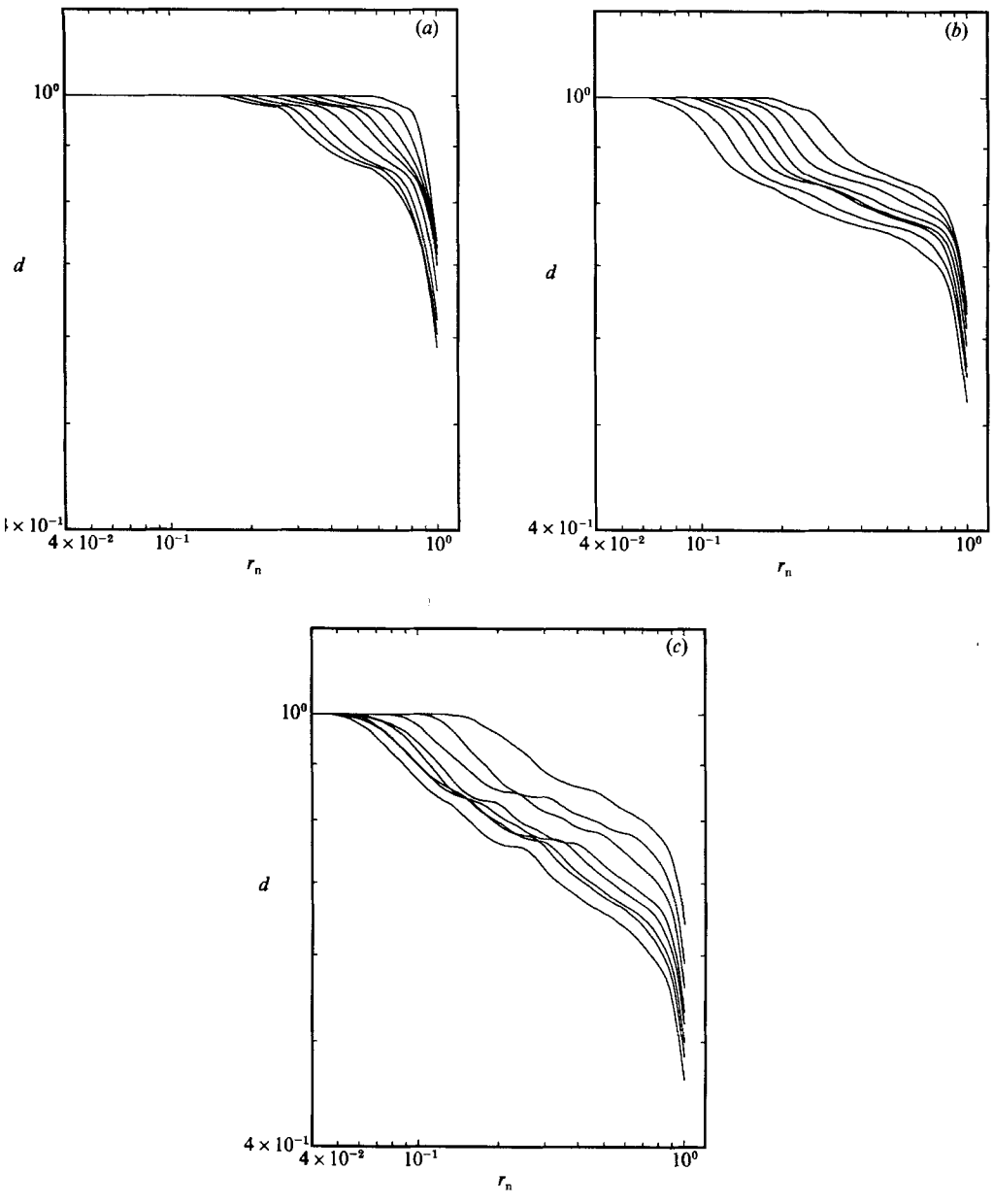

FIGURE 8. Sequence of d versus r_n curves for the immiscible fingering patterns shown in figures 1 (*a*), 1 (*b*) and 1 (*c*) at (*a*) $\mu q/\gamma b^2 = 1.30$, (*b*) 4.99 and (*c*) 19.0. Each curve corresponds to each pattern shown in the respective figure, and the time for each curve can be found in the caption of figure 1, and time increases from the upper-right corner to the lower-left corner.

It is not clear why d_1 correlates with $(qt/b^3)(\mu q/\gamma b^2)$ but not with qt/b^3 and $(qt/b^3)(\mu q/\gamma b^2)^2$. In view of the correlations between the finger length with the last two dimensionless times (see figures 5 and 6), a simple argument suggests that d_1 should correlate with them, but plots (not shown) of d_1 against these two dimensionless times show that there is none.

A typical set of d–r_n curves for the miscible pattern is shown in figure 11. Similarly

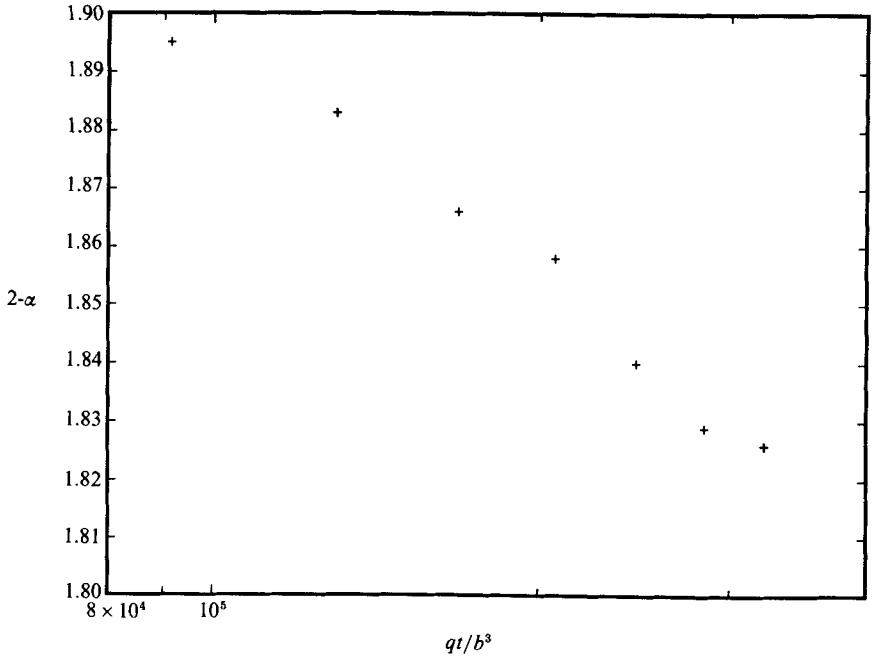

FIGURE 9. Value of $2-\alpha$ as a function of qt/b^3 for the last seven patterns shown in figure 1(*c*).

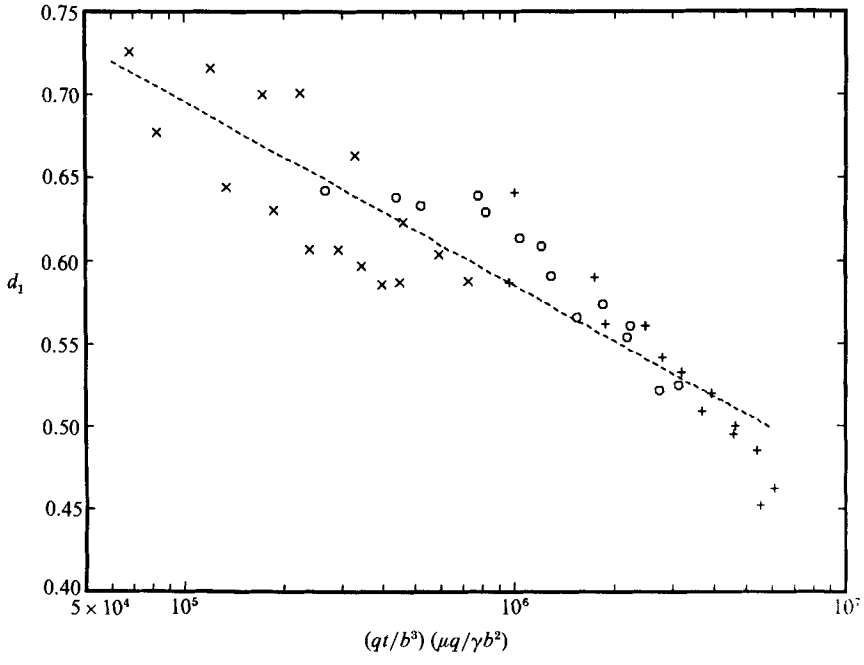

FIGURE 10. Overall density d_1 as a function of $(qt/b^3)(\mu q/\gamma b^2)$ for two runs at each flow rate, $\mu q/\gamma b^2 = 1.30$ (×), 4.99 (○) and 19.0 (+). Dashed line represents equation (11).

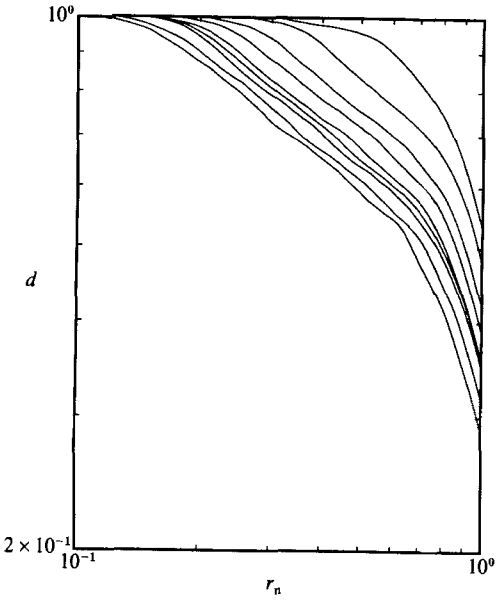

FIGURE 11. Sequence of d versus r_n curves for miscible fingering patterns at $q = 1.40\times10^{-4}$ ml/s ($q/Db = 9.3\times10^5$) at $t = 28$, 68, 108, 148, 188, 228, 268, 359 and 459 s. The time of each curve increases from the upper-right corner to the lower-left corner. Patterns at $t = 228$ and 459 s are shown in figure 3.

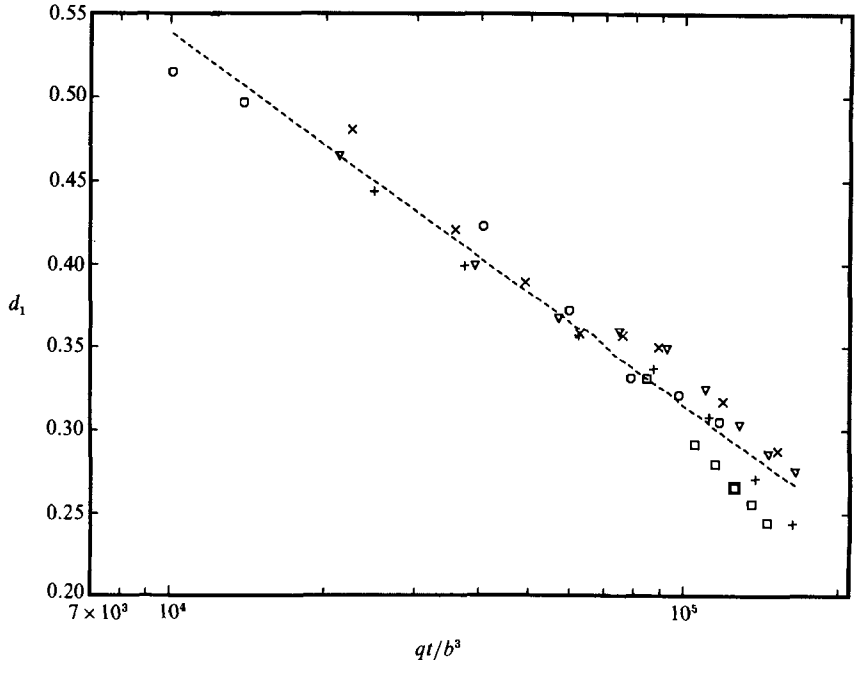

FIGURE 12. Overall density d_1 as a function of qt/b^3 at $q/Db = 4.75\times10^5$ (□), 9.3×10^5 (×), 3.57×10^6 (○), 5.0×10^6 (▽), 7.0×10^6 (+). Dashed line represents equation (12).

to the immiscible case, the d–r_n curve shifts towards the lower-left corner of the figure as time increases. At late stages the intermediate portion of the curves becomes a roughly parallel straight line with slope $-\alpha$ in a log–log plot. The lines are straighter than those shown in figure 8 for the immiscible patterns, where the number of splittings is much less and the sizes of fingers are much bigger than those of the miscible patterns. At later stages (roughly more than ten generations of splitting) the value of $-\alpha$ reaches a constant. Analysis of patterns developed at other flow rates shows the same behaviour. This means that the fingering pattern becomes more and more sparse as it grows through splitting, and is a fractal object provided that there is enough splitting. For the five flow rates tested the values of α are 0.50, 0.43, 0.42 (0.41), 0.42 and 0.45 in order of increasing flow rate. The value in parentheses is for the second run at $q = 5.35 \times 10^{-4}$ ml/s. This means that the fractal dimension, $2-\alpha$, of miscible fingering patterns ranges from 1.69 to 1.50 and is insensitive to the flow rates tested. For radial water fingering patterns in a non-Newtonian aqueous polymer solution, Daccord *et al.* (1986) find that the fractal dimension ranges from 1.65 to 1.75.

Figure 12 summarizes d_1 for miscible patterns at different times for the five flow rates tested. The dashed line in the figure represents the least-square-fit to the data,

$$d_1 = 1.43 - 0.097 \ln\left(\frac{qt}{b^3}\right). \tag{12}$$

Somewhat similarly to the immiscible case, d_1 correlates with qt/b^3 but not with $(qt/b^3)(q/Db)$ or $(qt/b^3)(q/Db)^2$.

3.4. *Splitting wavelength*

For each experiment, time-sequence photographs are examined and the splitting wavelength, λ, is identified as the maximum-to-maximum distance of the earliest discernible indentation on a finger tip. For each such indentation of the immiscible finger three repeated measurements of the distance are made and for all data the maximum error is $\pm 5\%$ of the average value of three measurements. The finger speed V at the moment, t, of discernible indentation is the average of the speeds of the two new fingers. The speed of each new finger is calculated from

$$(r_t(t+\delta t) - r_t(t-\delta t))/2\delta t,$$

where δt is the time interval between two consecutive photographs. For all data the speed of the new finger is within 7% of the finger speed V.

In figure 13 we compare our λ/b versus Ca data with the results of linear stability analyses and experimental data available in the literature. It is useful to refer to figure 1 when reading the data in figure 13. Data from two runs at each flow rate are shown. Each symbol represents data collected from each flow rate. In each group of each symbol the data at higher Ca roughly corresponds to an earlier generation of splitting, since for constant flow rate the finger speed is larger when the pattern is smaller. The chain-dashed line in figure 13 is the least-square-fit to our data,

$$\frac{\lambda}{b} = 8.7 Ca^{-0.31} \tag{13}$$

for Ca ranging from 0.0008 to 0.05. The fact that λ/b scales with $Ca^{-0.31}$, instead of $Ca^{-0.5}$ as predicted by linear stability analyses for a planar interface, shows that the finger curvature plays a role in the splitting. This stabilizing effect of finger curvature

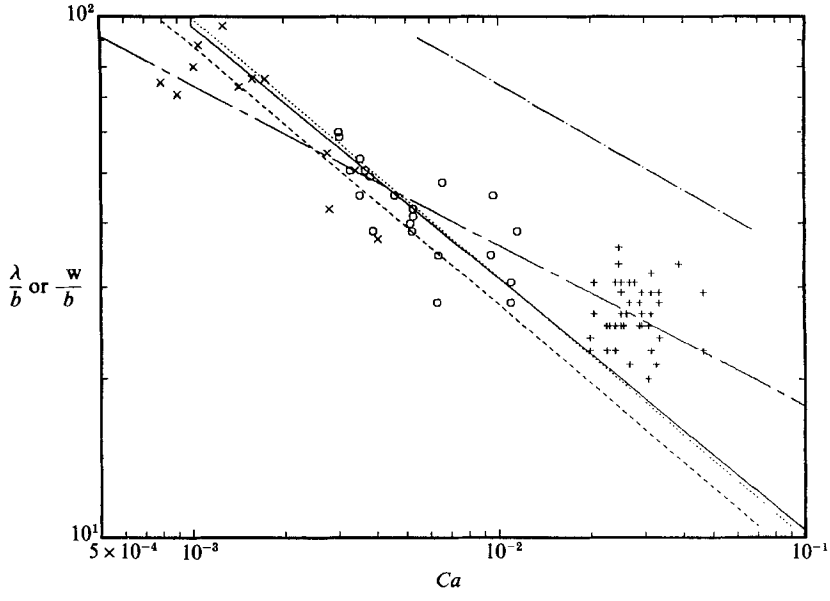

FIGURE 13. Comparison between linear stability analyses and experimental data (λ/b or w/b) as functions of Ca for immiscible fingers. Our data from two runs at each flow rate are shown: $\mu q/\gamma b^2 = 1.30$ (×), 4.99 (○) and 19.0 (+). Chain-dashed line and chain-dotted line, respectively, represent the least-square-fits to our λ/b data, equation (13), and Kopf-Sill & Homsy's (1988) w/b data. Dotted, dashed and solid lines represent theoretical results from equations (14), (15) and (16), respectively.

on splitting has been reported by Kopf-Sill & Homsy (1988) on experiments for long fingers in a linear cell. The chain-dotted line in figure 13 represents the (w/b)–Ca relationship reduced from the least-square-fit result presented in their figure 12. Here w is the average finger width, which is a measure of the splitting wavelength λ. w is larger than λ, because λ is measured at the beginning of splitting and w is measured when the splitting is complete (see Kopf-Sill & Homsy 1988 for the definition of w). Their results show that the average finger width scales with $Ca^{-0.35}$ for $0.0055 < Ca < 0.08$.

It is also interesting to compare our results with linear stability analyses. In figure 13 the dotted line represents

$$\frac{\lambda}{b} = \pi Ca^{-\frac{1}{2}}, \tag{14}$$

the dashed line represents

$$\frac{\lambda}{b} = 2.78 Ca^{-\frac{1}{2}}, \tag{15}$$

and the solid line represents the (λ/b)–Ca relationship (Schwartz 1986) obtained from the positive real root of

$$\left(\frac{\pi J}{216}\right) Ca^{\frac{1}{6}} \left(\frac{2\pi}{\Lambda}\right)^3 + \left(\frac{\pi}{16}\right)\left(\frac{2\pi}{\Lambda}\right)^2 - 1 = 0, \tag{16}$$

where J is 3.8 and $\Lambda \equiv (\lambda/b)\, Ca^{\frac{1}{2}}$. Equation (14) is derived (Saffman & Taylor 1958; Chuoke *et al.* 1959; Paterson 1981) based on the following boundary condition:

$$p_i - p = \gamma\left(\frac{2}{b} + \frac{1}{a}\right). \tag{17}$$

Equation (16) is obtained by Schwartz (1986) from a linear stability analysis for a planar interface, using a more appropriate boundary condition for the pressure jump derived by Park & Homsy (1984):

$$p_i - p = \gamma\left(\frac{2}{b} + \frac{\pi}{4a}\right) + \frac{2\gamma J}{b} Ca^{\frac{2}{3}}. \tag{18}$$

Here a is the radius of curvature of the projection of the interface on the plate. This boundary condition is valid for small Ca and considers the effects of the wetting film and of the three-dimensionality near the interface. When there is no wetting film or in the limit of zero Ca, (16) reduces to (15) (Schwartz 1986). It is clear from figure 13 that these linear stability analyses for a planar interface fail to predict the smaller slopes in Kopf-Sill & Homsy's data and ours. It is interesting to note that the boundary condition proposed by Park & Homsy (1984) seems to correct the slope in the right direction, as shown by the solid line in figure 13 for the results of Schwartz (1986). No theoretical calculations that include the effects of tip curvature and finger interaction are available for comparison with the experimental data. Numerical calculations on the evolution and stability of a long finger have been reported by DeGregoria & Schwartz (1985). Numerical calculations on the interaction of multiple fingers and the evolution of fingering patterns have been done by Tryggvason & Aref (1983, 1985).

For miscible fingers, the wavelength, λ, at splitting is not sensitive to the flow rates tested. For each experiment λ is measured for at least nine splitting fingers. In order of decreasing flow rate, the mean and standard deviations of λ are 0.048 ± 0.008, 0.057 ± 0.012, 0.047 ± 0.006, 0.064 ± 0.017, 0.066 ± 0.011 cm. This means that λ ranges from $5b$ to $10b$ and is not sensitive to the flow rates tested. And its value is larger than the $4b$ predicted by the linear stability analysis of Paterson (1985). Note that the comparisons are not exact, since the data are obtained from long fingers and the linear stability analysis is based on a circular interface. In addition, the fingers are not of uniform thickness, whereas the linear stability analysis assumes a uniform thickness (Paterson 1985). Paterson showed in his experiments that many of the incipient fingers appeared to have a wavelength of $4b$, where $b = 0.15$ and 0.3 cm and q/Db ranges from about 10^7 to 10^8. In our experiment $b = 0.0075$ cm and $q/Db = 4.8 \times 10^5$–7.0×10^6. Daccord *et al.* (1986) reported a finger width of $4.6b$ for b ranging from 0.02 to 0.12 cm when water radially fingers into a non-Newtonian aqueous polymer solution. Our data suggest that for large dimensionless flow rate q/Db, the value of λ/b is insensitive to dispersion and ranges from 5 to 10.

4. Summary

A series of experiments on miscible and immiscible viscous fingering has been carried out. The displaced fluid is glycerine of viscosity 1050 cP and the displacing fluid is either miscible (water) or immiscible (oil) with glycerine, with viscosity 1.0 cP. The data presented in this paper are taken mostly at late stages of finger growth when the pattern has multiple generations of splitting. In §3.1 we find a geometrical similarity between immiscible patterns at the same generation of splitting. This finding is confirmed quantitatively in §3.2. We also show that the miscible patterns are insensitive to dispersion for large q/Db. In §3.2 we find correlations between the finger length and time. In particular we estblish the correct length- and timescales for the immiscible pattern. We show that two immiscible patterns are geometrically similar at the same dimensionless time, if the correct length- and timescales are used.

This observation also shows that at the same dimensionless time the two similar patterns have the same generation of splitting. We suggest that the generation of splitting is a good indication of the 'age' of the pattern. In §3.3 we find that the pattern has to go through a certain number of generations of splitting before it shows fractal behaviour. Our data for the immiscible pattern show that the fractal dimension, $2-\alpha$, decreases from 1.9 to 1.82 when the pattern goes from the third to the sixth generation of splitting. Further experiment is needed to check whether the value of $2-\alpha$ will reach a constant, what the constant is, and at which generation of splitting it reaches this constant. Our data for the miscible pattern show that the fractal dimension reaches a constant when the pattern has more than ten generations of splitting. The constant value ranges from 1.50 to 1.69 and is insensitive to the flow rates tested, $q/Db = 4.8 \times 10^5$–7.0×10^6. In §3.4 we find that for the immiscible finger λ/b scales with $Ca^{-0.31}$. The exponent, -0.31, is close to that of -0.35 obtained by Kopf-Sill & Homsy (1988) for long fingers in a linear cell. This is in agreement with their observation that the finger tip curvature stabilizes the finger. For the miscible finger the value of λ/b is insensitive to dispersion and ranges from 5 to 10 for large q/Db.

I thank J. B. Roberts and B. Schmidt for their help with the data collection. I also thank the referees for their useful criticisms on the manuscript of this paper. This work was performed at Schlumberger-Doll Research, Old Quarry Road, Ridgefield, CT 06877-4108.

REFERENCES

Benham, A. L. & Olson, R. W. 1963 A model study of viscous fingering. *Soc. Petrol. Engng J.* 138–144.

Blackwell, R. J., Rayne, J. R. & Terry, W. M. 1959 Factors influencing the efficiency of miscible displacement. *Petrol. Trans. AIME* **216**, 1–8.

Burnett, L. J. & Harmon, J. F. 1972 Self-diffusion in viscous liquids: pulse NMR measurements. *J. Chem. Phys.* **57**, 1293–1297.

Chen, J. D. 1987 Radial viscous fingering patterns in Hele-Shaw cells. *Exp. Fluids* **5**, 363–371.

Chouke, R. L., van Meurs, P. & van der Poel, C. 1959 The instability of slow, immiscible, viscous liquid–liquid displacements in permeable media. *Petrol. Trans. AIME* **216**, 188–194.

Daccord, G., Nittmann, J. & Stanley, H. 1986 Radial viscous fingers and diffusion-limited aggregation. *Phys. Rev. Lett.* **56**, 336–339.

DeGregoria, A. J. & Schwartz, L. W. 1985 Finger breakup in Hele-Shaw cells. *Phys. Fluids* **28**, 2313–2314.

Hele-Shaw, H. S. 1898 The flow of water. *Nature* **58**, 34–36.

Homsy, G. M. 1987 Viscous fingering in porous media. *Ann. Rev. Fluid Mech.* **19**, 271–311.

Howard, G. C. & Fast, C. R. 1970 *Hydraulic Fracturing*. Soc. Petrol. Engng, AIME, Dallas, TX.

Howison, S. D. 1986 Fingering in Hele-Shaw cells. *J. Fluid Mech.* **167**, 439–453.

Kopf-Sill, A. R. & Homsy, G. M. 1988 Nonlinear unstable viscous fingers in Hele-Shaw flows. I. Experiments. *Phys. Fluids* **31**, 242–249.

Mandelbrot, M. M. 1983 *The Fractal Geometry of Nature*. San Francisco: Freeman.

Park, C. W. & Homsy, G. M. 1984 Two-phase displacement in Hele-Shaw cells: theory. *J. Fluid Mech.* **139**, 291–308.

Paterson, L. 1981 Radial fingering in a Hele-Shaw cell. *J. Fluid Mech.* **113**, 513–529.

Paterson, L. 1985 Fingering with miscible fluids in a Hele-Shaw cell. *Phys. Fluids* **28**, 26–30.

Rauseo, S. N., Barnes, P. D. & Maher, J. V. 1987 Development of radial fingering patterns. *Phys. Rev.* A **35**, 1245–1251.

SAFFMAN, P. G. & TAYLOR, G. I. 1958 The penetration of a fluid into a porous medium or Hele-Shaw cell containing a more viscous liquid. *Proc. R. Soc. Lond.* A **245**, 312–329.

SCHWARTZ, L. 1986 Stability of Hele-Shaw flows: The wetting layer effect. *Phys. Fluids* **29**, 3086–3088.

STALKUP, F. I. 1984 *Miscible Displacement*. Soc. Petrol. Engng, AIME, Dallas, TX.

TABELING, P., ZOCCHI, G. & LIBCHABER, A. 1987 An experimental study of the Saffman–Taylor instability. *J. Fluid Mech.* **177**, 67–82.

TRYGGVASON, G. & AREF, H. 1983 Numerical experiments on Hele-Shaw flow with a sharp interface. *J. Fluid Mech.* **136**, 1–30.

TRYGGVASON, G. & AREF, H. 1985 Finger-interaction mechanisms in stratified Hele-Shaw flow. *J. Fluid Mech.* **154**, 287–301.

VAN MEURS, P. 1957 The use of transparent three-dimensional models for studying the mechanism of flow process in oil reservoirs. *Trans. AIME* **210**, 295–301.

WITTEN, T. A. & SANDER, L. M. 1983 Diffusion-limited aggregation. *Phys. Rev.* B **27**, 5686–5697.